Order-determined structural and energy transport dynamics in solid-supported interfacial methanol

Xing He, Ding-Shyue Yang*

Department of Chemistry, University of Houston, Houston, Texas 77204 United States

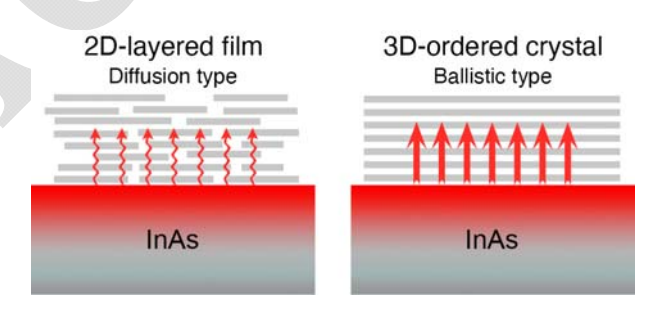
^{*}To whom correspondence should be addressed. Email: yang@uh.edu

Abstract

Energy transport dynamics in different nanostructures are crucial to both fundamental understanding and practical applications for heat management at the nanoscale. It has been reported that thermal conductivity may be severely impacted by stacking disorder in layered materials. Here, using ultrafast electron diffraction in the reflection geometry for direct probing of structural dynamics, we report a fundamental behavioral difference due to stacking order in an entirely different system—solid-supported methanol assemblies whose layered structures may resemble those of two-dimensional (2D) and van der Waals (vdW) solids but with much weaker in-plane hydrogen bonds. Thermal diffusion is found to be the transport mechanism across 2D-layered films without a cross-plane stacking order. In stark contrast, much faster ballistic energy transport is observed in 3D-ordered crystalline solids. The major change in such dynamical behavior may be associated with the efficiency of vibrational coupling between vdW-interacted methanol layers, which demonstrates a strong structure—property relation.

Keywords: interfacial energy transfer, cooperative molecular motions, scattering of cross-plane phonons, Debye-Waller, heat conduction

TOC Figure



Energy transport and thermal management have become critical subjects to consider as basic components in modern electronics are firmly in the nanoscale realm.¹⁻³ Because of the comparable phonon mean free paths and materials sizes, the transport mechanisms in nanostructures may exhibit features that are significantly different from those in the bulk described by the conventional Fourier's law of heat conduction, hence showing, e.g., interfacial effects,^{1, 3} phonon confinements,⁴ coherent phonon transport,⁵ and strong anisotropy in heat conduction.⁶ For different desired thermal performances or even new optoelectronic functions on the nanoscale, incorporation of various materials with different structures has been contemplated, including two-dimensional (2D) or nanostructures for micro- and optoelectronic devices,^{7, 8} thermoelectric materials for energy conversion,⁹ and thermal barrier coatings.¹⁰ Due to these reasons and many others, the discoveries of 2D materials and van der Waals (vdW) solids have led to tremendous attention and amount of research considering their unique structures and novel properties.^{11, 12}

It is known that 2D and layered materials may exhibit significantly anisotropic thermal conductivities given stronger in-plane chemical bonds and much weaker interplanar interactions. However, the stacking order in a solid may further affect thermal conduction in a prominent way. It has been found that WSe₂ with disorderly stacked sheets exhibits a reduction in the cross-plane thermal conductivity by 30 times compared to that of an ordered, layered single crystal. In addition, the in-plane thermal conductivity of disordered WSe₂ is reduced by 6 times due to the smaller size of the crystalline sheets. In Interestingly, a disruption of the crystalline order by energetic ion bombardments can lead to an increase in the cross-plane thermal conductivity, which appears to be a remarkable finding and has structure–property implications. In

Such order-impacted transport behavior is not only limited to inorganic solids.¹⁸ Recently, a metastable, 2D-layered structure for the assembly of methanol molecules was reported,¹⁹ with hydrogen bonds within the long-range crystalline sheets and interplanar vdW interactions yet without an ordered stacking along the cross-plane direction. The 3D-ordered solid methanol can be obtained by further annealing the 2D assembly at an elevated temperature to facilitate the stacking alignment of the hydrogen-bonded sheets and form the crystal structure.¹⁹ In such a system, the difference between the strengths of hydrogen bonds and vdW interactions per molecule is considerably reduced compared to that of other systems with strong in-plane covalent/ionic bonds. Furthermore, hydrogen bonds and vdW interaction are crucial components in biological macromolecular systems, and an understanding of energy transport in structures containing these intermolecular interactions and resembling orders is needed. Thus, assemblies of methanol molecules can serve as a good model system to investigate the impact of structural orders on energy transport dynamics.

In this report, the energy transport processes in both 2D-layered and 3D-ordered methanol assembly structures are elucidated using ultrafast electron diffraction (UED). A drastic difference in the transport mechanism is found for films of different orders, where a fast ballistic propagation is observed for 3D-ordered crystalline films but a diffusion-type result for the 2D-layered structure. This contrast indicates the determining role of the cross-plane stacking on energy transport and thermal conductivity even though the structural differences may seem subtle, considering from a thermodynamic energy point of view regarding the strength of vdW interactions. Thus, the current study with molecular assemblies may have further implications in nanoscale structure-property relations for a broad range of materials and biological systems.

Diffractions of two ordered methanol assembly structures. Shown in Figure 1a-d are the

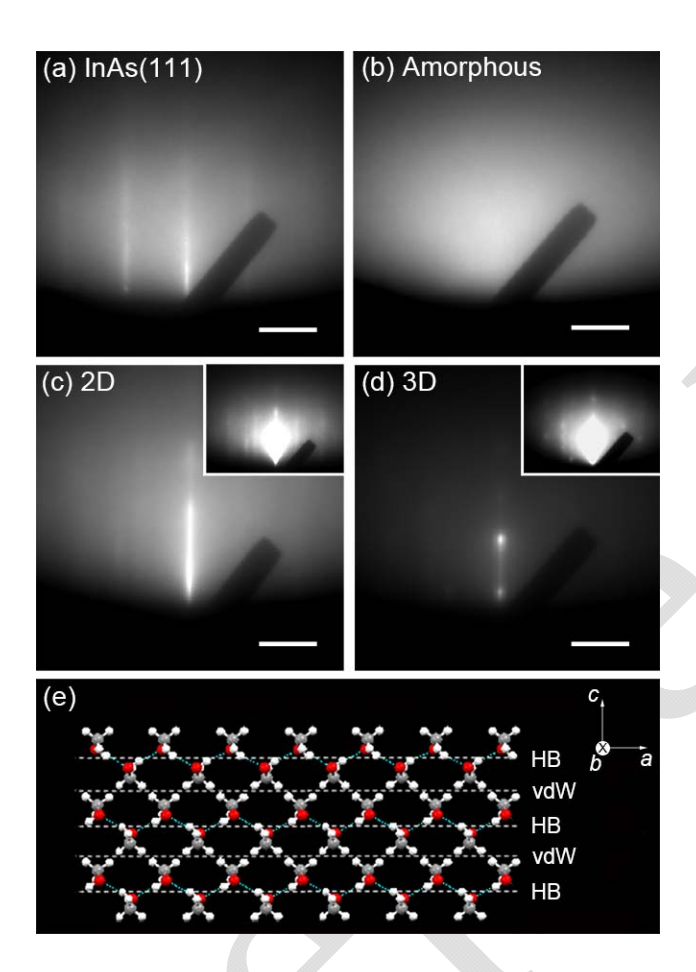


Figure 1. Diffraction images recorded from (a) bare InAs(111)A, (b) an as-deposited methanol film, (c) 2D-layered assembly, and (d) 3D crystalline structure. The insets show the same diffraction patterns with a lower intensity threshold to highlight the less intense side streaks or spots. The scale bars in a-d indicate a momentum transfer of 0.25 Å⁻¹. (e) Structure of 3D-ordered crystalline methanol (oxygen in red, carbon in grey, and hydrogen in white), showing layers of hydrogen-bonded chains (HB) and interlayer vdW interaction.

diffraction images recorded from a smooth supporting InAs(111)A substrate and interfacial methanol of three different structures (see Supporting Information for Experimental Section). During the first-stage crystallization, a 2D-layered assembly was gradually formed of asdeposited amorphous methanol (Figure 1b) at a temperature above 112 K¹⁹ and then stabilized

without further structural change by lowering the surface temperature back to ~100 K for UED measurements. The completion of the process was confirmed by the observation of clear diffraction streaks with stable intensities over time (Figure 1c). A 3D-ordered crystalline methanol film was obtained by raising the annealing temperature to 130 K and maintaining it for more than one hour until well-defined diffraction spots were observed (Figure 1d); the final film thickness after the inevitable but minor evaporation loss was determined by laser interferometry. The temperature was then lowered to ~100 K and the crystalline film was maintained without further change for UED measurements. The Bragg spots of 3D crystalline films indicate a long-range order in the vertical stacking of hydrogen-bonded methanol layers along the surface normal direction (Figure 1e), which is lacking in 2D-layered assemblies. In addition, by comparing the horizontal widths of the diffraction features, the lower values for 3D-ordered films also signify a better in-plane order from a larger average domain size compared to that of 2D-ordered assemblies. The surface of the diffraction features are compared to that of 2D-ordered assemblies.

Hence, the structures of 2D- and 3D-ordered methanol assemblies are reminiscent of those of WSe_2 reported earlier, ¹⁶ although the nature and strength of the in-plane bonding is significantly different.

Structural dynamics of 2D-layered methanol assemblies. Upon the impingement of a 1030-nm (i.e., 1.20-eV) laser pulse, the supporting InAs substrate undergoes an above-gap photoexcitation followed by heating of the lattice due to the excess energy released by photocarriers via electron-phonon coupling (see Supporting Information for Experimental Section and further description about the induced temperature jump).^{20, 21} Hence, effectively, a fast temperature jump is generated within several picoseconds (ps) in the top region of InAs, with surface atoms exhibiting enlarged vibrational motions. Such atomic movements along the

surface normal direction then affect the overlaying methanol molecules with vdW contacts, resulting in the subsequent energy transport across the interface. This cross-interface transport takes place over an extended duration because the effective temperature of the substrate surface remains elevated for at least a nanosecond (ns) time, owing to a rather large penetration depth of ~680 nm at 1.20 eV (from the absorption coefficient of 1.48×10⁴ cm⁻¹)²² and consequently slower heat dissipation into the bulk. As a result, the nonequilibrium structural dynamics is not of a ps impulse type but continue to build up and propagate through a methanol assembly toward the top of the film probed by UED in the reflection geometry (see below).

Given that no structural transition exists at the temperature and excitation fluences used, the reduction in the diffraction intensity is caused by the increased thermal motions of methanol molecules. Particularly, the intensity decrease of the center streak (Figure 2a) may be described by the Debye–Waller mechanism as follows:

$$\ln(I_0/I(t)) = 2W(t) = \Delta \langle (\vec{q} \cdot \vec{u}(t))^2 \rangle = 4\pi^2 s_\perp^2 \cdot \Delta \langle u_\perp^2(t) \rangle \tag{1}$$

where the I_0 and I(t) are, respectively, the diffraction intensities before the zero of time and at time t after photoexcitation, W the Debye–Waller factor, \vec{u} the atomic or molecular displacement vector, $\vec{q} = 2\pi \vec{s}_{\perp}$ the scattering vector, and $s_{\perp} = 2\sin(\theta/2)/\lambda$ the vertical momentum transfer along the surface normal direction, with θ being the total scattering angle and $\lambda = 0.0698$ Å the de Broglie wavelength of 30-keV electrons. $\Delta \langle u_{\perp}^2(t) \rangle$ is the change in the out-of-plane component of the mean-square displacements (MSD). Thus, the good linear relation between $\ln(I_0/I(t))$ and s_{\perp}^2 supports the structural origin of the observed diffraction changes, whose slope gives $4\pi^2\Delta \langle u_{\perp}^2(t) \rangle$ (Figure 2b). The linear dependence of $\Delta \langle u_{\perp}^2 \rangle$ on the laser fluence used is anticipated for one-photon photoexcitation and therefore a linear heating scenario (Figure 2c). We also note the lack of notable intensity changes near the shadow edge (Figure 2a), which

rules out the possibility of significant transient surface electric fields as the explanation for the observed diffraction changes (see Supporting Information).²³

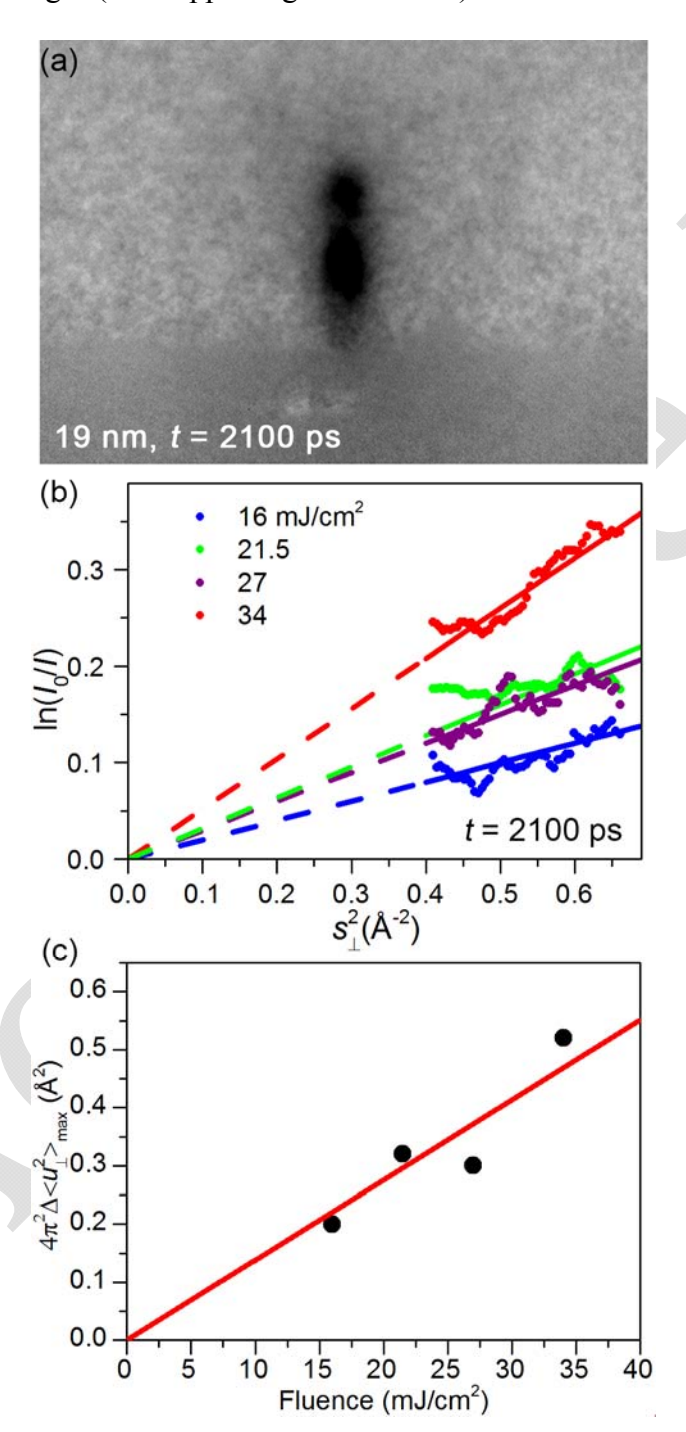


Figure 2. Structural dynamics of 2D-layered, 19-nm-thick methanol film. (a) Diffraction difference image at t = 2100 ps referenced to a negative-time frame before excitation. (b)

Diffraction intensity changes along the center streak as a function of s_{\perp}^2 at t=2100ps, at different laser fluences used. The symbols are the experimental results obtained via fit of a Gaussian function to the horizontal intensity curve at each s_{\perp} , and the lines are linear fits according to Equation 1. (c) Increase in the maximum of mean-square molecular displacements, $\Delta \langle u_{\perp}^2 \rangle_{\rm max}$, as a function of the excitation fluence. The solid line is a linear fit.

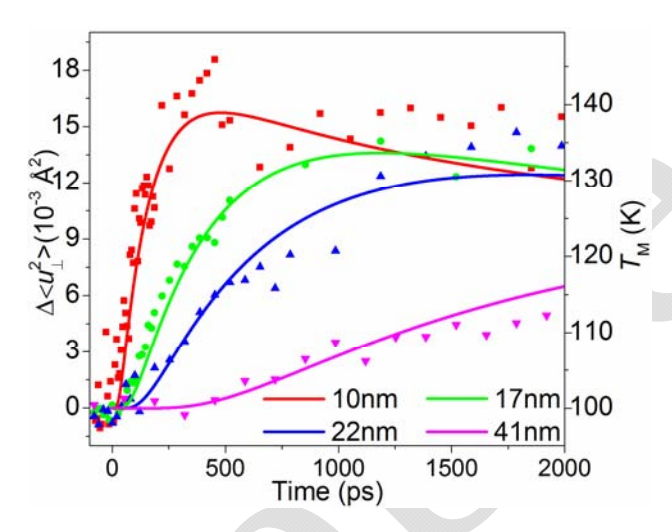


Figure 3. Temporal dependence of MSD increases at the top of methanol films with different thicknesses after photoexcitation of the supporting InAs substrate. The laser fluence used was 41.6 mJ/cm². The solid lines are the results simulated based on the described diffusion model, with the effective temperatures at the top of methanol assemblies as shown on the right axis.

Because the elastic mean free path of 30-keV electrons in methanol is about 108 nm, only the layers within the top few nm are probed at the grazing incidence of \sim 1°. Thus, time-dependent experiments conducted with different film thicknesses allow the examination of the structural dynamics of 2D methanol assemblies at different distances above the solid–molecule interface. Shown in Figure 3 are the out-of-plane MSD increases observed from films of different thicknesses (d = 10 to 41 nm) following laser excitation of the substrate, which may be further associated with temperature increases. The following phenomenological findings are

remarkable. As the thickness of a 2D-layered film increases, even by a few nm only, the out-of-plane MSD rise time becomes significantly prolonged. Furthermore, an apparent delay for the onset of change is observed and becomes appreciably larger for a thicker film. Concurrently, the amount of the out-of-plane MSD increase is reduced on the sub-ns time scale. These trends of the MSD dynamics appear to be unusual considering that the change in the film thickness is in the nanometer range, compared to the sub- μ m to μ m-thick heated substrate region. However, it may be reasonable to consider that a thermal diffusion process is at work for the temporal dependence of $\Delta \langle u_{\perp}^2 \rangle$, according to the time scale involved in Figure 3. As an example, using the time of $t_{\text{max}} \sim 300$ ps to reach the maximum of $\Delta \langle u_{\perp}^2 \rangle$ for a 10-nm-thick 2D-layered film (Figure 3, red), we estimate the thermal conductivity of solid methanol $K_{\text{M}} \cong \rho_{\text{M}} c_{\text{p,M}} (d^2/t_{\text{max}}) \approx 0.46$ W/(m·K) with the density $\rho_{\text{M}} = 1.028$ g/cm³ ²⁴ and specific heat $c_{\text{p,M}} = 1.34$ J/(g·K) at 100 K²⁵ for crystalline methanol, which is in a good agreement with the literature.

To be more quantitative, a heat diffusion model is used to simulate the temperature of a methanol film, $T_{\rm M}(z_{\rm M},t)$, as a function of time and distance $z_{\rm M}$ from the substrate surface, which includes an impulse heating of the InAs substrate considering volume generation of heat,²⁷ the energy transport from the heated substrate to the molecular film across the interface due to atomic motions, and the upward thermal diffusion with $K_{\rm M}=0.36~{\rm W/(m\cdot K)}$:²⁶

$$\frac{\partial^2 T_{M}(z_{M},t)}{\partial z^2} - \frac{\rho_{M} c_{p,M}}{K_{M}} \frac{\partial T_{M}(z_{M},t)}{\partial t} = 0$$
 (2)

$$T_{\mathbf{M}}(z_{\mathbf{M}},0) = T_{\mathbf{0}} \tag{3}$$

where T_0 is the substrate temperature without laser excitation. However, instead of equating the temperatures at the interface as the boundary condition, we consider the vibrating surface atoms of heated InAs and the immediate interfacial layer of methanol molecules to have the same average displacement increase along the surface normal direction,

$$\Delta \langle u_{\perp,\mathrm{M}}^2(0,t) \rangle^{1/2} = \Delta \langle u_{\perp,\mathrm{InAs}}^2(0,t) \rangle^{1/2}. \tag{4}$$

This is physically more reasonable than the use of the same temperature considering what actually happens at the solid-molecule interface and how atomic movements at the substrate surface affect adjacent molecules that have only vdW contacts. Then each $\Delta \langle u_{\perp,M}^2(0,t) \rangle^{1/2}$ value for methanol corresponds to an equivalent $T_{\rm M}(0,t)$ for diffusion simulation (see Supporting Information for further details).

The simulated curves of the effective temperature at the top layer of the methanol films are shown as solid lines in Figure 3. With only a single universal factor to match the amplitude of change, a good agreement is reached between the simulated results and the experimental data for all thicknesses measured, including the time dependence and the delayed onset of change. Thus, it is concluded that thermal diffusion is the energy transport mechanism at work across a 2D-layered methanol thin film, with thermal conductivity similar to that of the crystalline bulk.

Structural dynamics of 3D crystalline methanol. Structurally, as mentioned above, interfacial methanol with the 3D crystalline structure exhibits a longer-range order in both in-plane and cross-plane directions, in contrast with that of a 2D-layered assembly. Dynamically, major differences are also found in the time-resolved structural dynamics of 3D crystalline films compared to those of the 2D-layered structure (Figure 4). In fact, the temporal dependence of diffraction change of a 3D-ordered film resembles that of the laser-excited supporting substrate, which is in stark contrast with the slow rise of the out-of-plane MSD increase observed from a thick 2D-layered film as a result of the diffusion-type thermal conduction. We note that the out-of-plane MSD increases at the top layers of 22- and 100-nm-thick 3D crystalline films reach the maximum extent on the ps time scale following the temperature jump of the substrate surface.

Furthermore, the decay of a significant fraction of the MSD increase appears within ~100 ps, a trend that is opposite to the slow rise in hundreds of ps seen in 2D-layered assemblies (Figure 4).

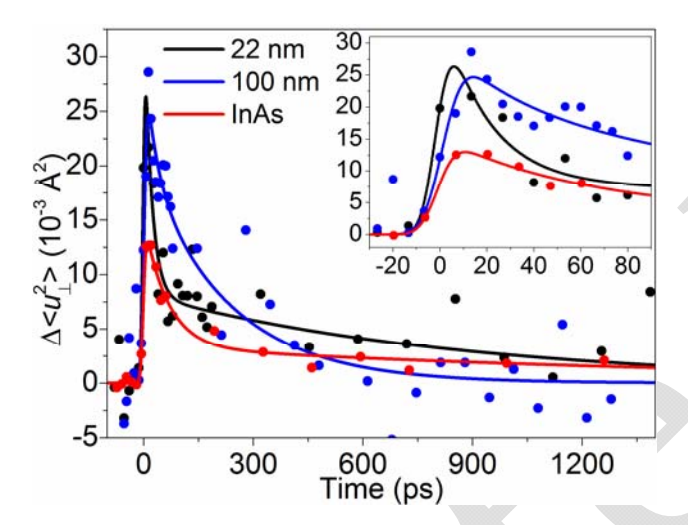


Figure 4. Comparison of MSD increases for 22-nm and 100-nm-thick 3D crystalline films and a bare InAs surface, at the laser fluence of 41.6 mJ/cm². The inset shows the dynamics at early times.

Given the same experimental conditions (except for the structural orders of the films), such drastic dynamical differences between 2D-layered and 3D-ordered cases cannot be dismissed merely by transient surface electric field effects. In fact, the observations signify a much faster energy transport in the 3D crystalline structure with a mechanism different from diffusion. The following points provide a consistent picture. First, for a faster rise and decay, it is reasonable to consider energy transport via phonons or ballistic propagation, therefore in a more coherent fashion than diffusion. Indeed, with the sound speed of about 2.80 km/s, ²⁸ the MSD rise times are expected to be of the order of 10 ps and slower for a 100-nm-thick film compared to a 22-nm-thick film (Figure 4). Second, because of the better layer-to-layer packing and hence less phonon scattering, the MSD decay under a coherent transport should follow the dynamics of the InAs surface, as energy dissipates toward the bulk in the reversed direction at longer times when

the supporting substrate gradually cools down. Third, it is also reasonable to see a similar level of $\Delta\langle u_\perp^2\rangle$ at early times at the top of films of different thicknesses as a result of coherent motions, whose value falls on sub-ns time below the threshold for quick thermodynamic evaporation loss. Lastly, at longer times, the recovery of $\Delta\langle u_\perp^2\rangle$ may eventually exhibit more thickness-dependent differences considering the finite size for wave-like propagation, structural anharmonicity for non-coherent motions, and thermalization across a film.

Relation between structures and energy transport. It is evident from the aforementioned results that changes in molecular assembly structures have profound impacts on their dynamical properties although they are composed of the same chemical component. Generally speaking, amorphous or glassy solids have low thermal conductivities compared to their crystalline counterparts because of the strong localization nature of heat carriers as a result of disordered structures.^{29, 30} In contrast, a well-ordered crystalline structure has delocalized propagating modes to contribute to a higher thermal conductivity.²⁹ However, the situation may be less apparent when both order and disorder (or misfits) are present in a solid, which becomes relevant in vdW materials and heterostructures.³¹⁻³⁴ In the WSe₂ studies mentioned earlier, a multilayered solid with disorder in the stacking exhibits a much lower cross-plane thermal conductivity compared to a well-stacked crystalline one.^{16, 17} Reduced thermal conductivities were also reported in another study of multi-component layered materials with structural misfits.³¹

In the present study, the distinct difference in the energy transport mechanism observed in the dynamics of the solid-methanol system is remarkable and may even be surprising for a number of reasons. First, to our best knowledge, this is the first molecular assembly system found by a direct structure-probing method (e.g., reflection UED in this study) to exhibit such

drastic dynamical behavioral differences, as a result of a seemingly small change in the stacking order. In fact, the contrast in the transport mechanisms could be considered greater than that found in ordered vs. disorderly-stacked WSe₂ with the similar diffusion process. ¹⁶ Second, both 2D-layered and 3D-ordered methanol assemblies have intralayer hydrogen bonds and cross-plane vdW interactions, although an in-plane domain size effect is anticipated for the former, and the latter between the two structures may likely have a small difference in energy per molecule. Two scenarios are possible to account for the observed difference in the mode of energy transport: (i) coherent cross-plane propagation or noncoherent diffusion is highly dependent on the lateral domain size, in that a more extended layer with many more methanol molecules favors synchronized movements whereas smaller domains with structural disorders in the boundaries disrupt coherent motions; (ii) compared to the 3D crystalline structure, the disorder and azimuthal rotation in the stacking of 2D-layered assemblies cause strong scattering or trapping of cross-plane energy-carrying phonons, resulting in a significant reduction in the transport speed and phenomenologically a different mode of energy transfer because of localization of the nonpropagating vibrational modes. 33, 34 It may also be possible that both scenarios contribute to our observations.

Third, the coherent cross-plane propagation of phonons in the 3D-ordered structure also signifies the preference of collective out-of-plane motions of hydrogen-bonded methanol molecules of the same layer, as well as a good structural coupling between layers even with vdW separation. These understandings give another example showing the cooperative nature of a hydrogen-bonded network (instead of unassociated individual molecular movements), which has been observed as the crucial underlying mechanism during a nonequilibrium phase transformation of ice in two solid–water systems.^{35, 36} Lastly, the similarity of thermal

conductivity between the 2D-layered structure and the bulk (likely polycrystalline) solid methanol is noted, ²⁶ which may provide a consistent picture for a heat diffusion process. By the argument of Chiritescu *et al.*, ¹⁶ the thermal conductivity of a 2D-layered assembly could be even lower than the bulk value. However, we also note a potential negative correlation between the inplane bonding strength and the cross-plane thermal conductivity described by Wei *et al.* ³⁷ Given the weak hydrogen bonds as the main in-plane intermolecular interaction, the disorder-induced reduction in the cross-plane thermal conductivity may be much less for methanol (thus maintaining the bulk value), compared to the significant reduction seen in the case of WSe₂ with more-than-one-order-of-magnitude stronger in-plane ionic bonds.

In conclusion, by using ultrafast electron diffraction in the reflection geometry, we have directly probed and resolved the structural dynamics and underlying energy transport mechanisms in solid-supported methanol assemblies, for both 2D-layered and 3D crystalline structures of different thicknesses. The structural order in the vdW stacking of hydrogen-bonded methanol layers was found to be the determining factor for the dynamical behavior. Because of the disorder and azimuthal misalignment in the stacking of the 2D-layered assembly, noncoherent heat diffusion from the laser-heated substrate surface to the top of the film is resulted, with prominent delays in the structural dynamics of slightly thicker films and a thermal conductivity similar to that of the bulk crystallized methanol. However, the ordered layer stacking and alignment as well as the enlarged lateral domain size in the 3D crystalline structure permit a much faster ballistic phonon propagation as the energy transport mechanism, as seen from the fast rise and recovery of the structural change at the top of a film resembling those of the substrate surface. The evident contrast observed in this solid-methanol system, the first for molecular assemblies, may find similarity in the large thermal conductivity difference seen in the

inorganic material of ordered vs. disordered WSe2. 16 Taken together, these examples may

provide further understanding about structural impacts on energy conduction in layered and vdW

materials as well as organic optoelectronic materials. Finally, from a broader perspective, it is

also crucial to examine energy transport dynamics and structure-property relations in a variety of

molecular systems with different intermolecular interactions and/or structural motifs; for

example, self-assembled monolayers with chemical bonds along the chains and lateral vdW

interactions may serve as another model system for comparison. 38, 39

ASSOCIATED CONTENT

Supporting Information

Experimental section, simulation of thermal diffusion across the solid-molecule interface and in

a methanol assembly, schematic diagram for the thermal diffusion simulation, table for

comparison of interferometry-determined nominal thicknesses and best values for simulation,

exclusion of transient surface electric fields as possible cause for diffraction changes

AUTHOR INFORMATION

Corresponding Author

*Email: <u>yang@uh.edu</u> Phone: +1 713-743-6022.

ORCID

Xing He: 0000-0001-5341-5662

Ding-Shyue Yang: 0000-0003-2713-9128

Notes

The authors declare no competing financial interest.

16

ACKNOWLEDGEMENTS

This research was supported by a National Science Foundation CAREER Award (CHE-1653903) and the R. A. Welch Foundation (E-1860).

REFERENCE

- 1. Cahill, D. G.; Ford, W. K.; Goodson, K. E.; Mahan, G. D.; Majumdar, A.; Maris, H. J.; Merlin, R.; Phillpot, S. R. Nanoscale thermal transport, *J. Appl. Phys.* **2003**, 93, 793-818.
- 2. Pop, E. Energy dissipation and transport in nanoscale devices, *Nano Res.* **2010**, 3, 147-169.
- 3. Cahill, D. G.; Braun, P. V.; Chen, G.; Clarke, D. R.; Fan, S.; Goodson, K. E.; Keblinski, P.; King, W. P.; Mahan, G. D.; Majumdar, A.; Maris, H. J.; Phillpot, S. R.; Pop, E.; Shi, L. Nanoscale thermal transport. II. 2003–2012, *Appl. Phys. Rev.* **2014**, 1, 011305.
- 4. Wang, Y.; Vallabhaneni, A.; Hu, J.; Qiu, B.; Chen, Y. P.; Ruan, X. Phonon lateral confinement enables thermal rectification in asymmetric single-material nanostructures, *Nano Lett.* **2014**, 14, 592-596.
- Luckyanova, M. N.; Garg, J.; Esfarjani, K.; Jandl, A.; Bulsara, M. T.; Schmidt, A. J.; Minnich, A. J.; Chen, S.; Dresselhaus, M. S.; Ren, Z.; Fitzgerald, E. A.; Chen, G. Coherent phonon heat conduction in superlattices, *Science* 2012, 338, 936-939.
- 6. Marconnet, A. M.; Panzer, M. A.; Goodson, K. E. Thermal conduction phenomena in carbon nanotubes and related nanostructured materials, *Rev. Mod. Phys.* **2013**, 85, 1295-1326.
- 7. Balandin, A. A. Thermal properties of graphene and nanostructured carbon materials, *Nat. Mater.* **2011**, 10, 569-581.
- 8. Yang, J.; Yang, Y.; Waltermire, S. W.; Wu, X.; Zhang, H.; Gutu, T.; Jiang, Y.; Chen, Y.; Zinn, A. A.; Prasher, R.; Xu, T. T.; Li, D. Enhanced and switchable nanoscale thermal conduction due to van der Waals interfaces, *Nat. Nanotechnol.* **2012**, *7*, 91-95.
- 9. Vineis, C. J.; Shakouri, A.; Majumdar, A.; Kanatzidis, M. G. Nanostructured thermoelectrics: big efficiency gains from small features, *Adv. Mater.* **2010**, 22, 3970-3980.
- 10. Padture, N. P.; Gell, M.; Jordan, E. H. Thermal barrier coatings for gas-turbine engine applications, *Science* **2002**, 296, 280-284.

- Butler, S. Z.; Hollen, S. M.; Cao, L. Y.; Cui, Y.; Gupta, J. A.; Gutiérrez, H. R.; Heinz, T. F.; Hong, S. S.; Huang, J. X.; Ismach, A. F.; Johnston-Halperin, E.; Kuno, M.; Plashnitsa, V. V.; Robinson, R. D.; Ruoff, R. S.; Salahuddin, S.; Shan, J.; Shi, L.; Spencer, M. G.; Terrones, M.; Windl, W.; Goldberger, J. E. Progress, challenges, and opportunities in two-dimensional materials beyond graphene, *ACS Nano* 2013, 7, 2898-2926.
- 12. Novoselov, K. S.; Mishchenko, A.; Carvalho, A.; Castro Neto, A. H. 2D materials and van der Waals heterostructures, *Science* **2016**, 353, aac9439.
- 13. Slack, G. A. Anisotropic thermal conductivity of pyrolytic graphite, *Phys. Rev.* **1962**, 127, 694-701.
- 14. McKinney, R.; Gorai, P.; Toberer, E. S.; Stevanovic, V. Rapid prediction of anisotropic lattice thermal conductivity: application to layered materials, *Chem. Mater.* **2019**, 31, 2048-2057.
- 15. Giri, A.; Chen, A. Z.; Mattoni, A.; Aryana, K.; Zhang, D.; Hu, X.; Lee, S.-H.; Choi, J. J.; Hopkins, P. E. Ultralow thermal conductivity of two-dimensional metal halide perovskites, *Nano Lett.* **2020**, 20, 3331-3337.
- Chiritescu, C.; Cahill, D. G.; Nguyen, N.; Johnson, D.; Bodapati, A.; Keblinski, P.; Zschack,
 P. Ultralow thermal conductivity in disordered, layered WSe₂ crystals, *Science* 2007, 315, 351.
- 17. Mavrokefalos, A.; Nguyen, N. T.; Pettes, M. T.; Johnson, D. C.; Shi, L. In-plane thermal conductivity of disordered layered WSe₂ and (W)_x(WSe₂)_y superlattice films, *Appl. Phys. Lett.* **2007**, 91, 171912.
- 18. Marinelli, M.; Mercuri, F.; Zammit, U.; Scudieri, F. Thermal conductivity and thermal diffusivity of the cyanobiphenyl (*n*CB) homologous series, *Phys. Rev. E* **1998**, 58, 5860-5866.
- 19. He, X.; Wu, C.; Yang, D.-S. Communication: No guidance needed: Ordered structures and transformations of thin methanol ice on hydrophobic surfaces, *J. Chem. Phys.* **2016**, 145, 171102.
- 20. Sundaram, S. K.; Mazur, E. Inducing and probing non-thermal transitions in semiconductors using femtosecond laser pulses, *Nat. Mater.* **2002**, 1, 217.
- 21. Yang, D.-S.; Gedik, N.; Zewail, A. H. Ultrafast electron crystallography. 1. nonequilibrium dynamics of nanometer-scale structures, *J. Phys. Chem. C* **2007**, 111, 4889-4919.

- 22. Adachi, S. Optical dispersion relations for GaP, GaAs, GaSb, InP, InAs, InSb, Al_xGa_{1-x}As, and In_{1-x}Ga_xAs_vP_{1-v}, *J. Appl. Phys.* **1989**, 66, 6030-6040.
- 23. He, X.; Chebl, M.; Yang, D.-S. Cross-examination of ultrafast structural, interfacial, and carrier dynamics of supported monolayer MoS₂, *Nano Lett.* **2020**, 20, 2026-2033.
- 24. Kirchner, M. T.; Das, D.; Boese, R. Cocrystallization with acetylene: molecular complex with methanol, *Cryst. Growth Des.* **2008**, 8, 763-765.
- 25. Sugisaki, M.; Suga, H.; Seki, S. Calorimetric study of the glassy state. III. novel type calorimeter for study of glassy state and heat capacity of glassy methanol, *Bull. Chem. Soc. Jpn.* **1968**, 41, 2586-2591.
- 26. Korolyuk, O. A.; Krivchikov, A. I.; Sharapova, I. V.; Romantsova, O. O. Heat transfer in solid methyl alcohol, *Low Temp. Phys.* **2009**, 35, 290-293.
- 27. Bechtel, J. H. Heating of solid targets with laser pulses, J. Appl. Phys. 1975, 45, 1585.
- 28. Srinivasan, A.; Bermejo, F. J.; de Bernabé, A. A Brillouin light-scattering investigation of the glass-transition in low molecular weight network glass-formers, *Mol. Phys.* **1996,** 87, 1439-1457.
- 29. Allen, P. B.; Feldman, J. L. Thermal conductivity of disordered harmonic solids, *Phys. Rev. B* **1993**, 48, 12581-12588.
- 30. Giri, A.; Donovan, B. F.; Hopkins, P. E. Localization of vibrational modes leads to reduced thermal conductivity of amorphous heterostructures, *Phys. Rev. Mater.* **2018**, 2, 056002.
- 31. Chiritescu, C.; Cahill, D. G.; Heideman, C.; Lin, Q.; Mortensen, C.; Nguyen, N. T.; Johnson, D.; Rostek, R.; Böttner, H. Low thermal conductivity in nanoscale layered materials synthesized by the method of modulated elemental reactants, *J. Appl. Phys.* **2008**, 104, 033533.
- 32. Wan, C.; Wang, Y.; Norimatsu, W.; Kusunoki, M.; Koumoto, K. Nanoscale stacking faults induced low thermal conductivity in thermoelectric layered metal sulfides, *Appl. Phys. Lett.* **2012**, 100, 101913.
- 33. Muratore, C.; Varshney, V.; Gengler, J. J.; Hu, J. J.; Bultman, J. E.; Smith, T. M.; Shamberger, P. J.; Qiu, B.; Ruan, X.; Roy, A. K.; Voevodin, A. A. Cross-plane thermal properties of transition metal dichalcogenides, *Appl. Phys. Lett.* **2013**, 102, 081604.

- 34. Ju, H.; Jeong, D.-G.; Choi, Y.-G.; Son, S.; Jung, W.-G.; Jung, M.-C.; Kang, S.; Han, M. J.; Kim, B.-J.; Park, J.-G.; Lee, J. S. Influence of stacking disorder on cross-plane thermal transport properties in TMPS₃ (TM = Mn, Ni, Fe), *Appl. Phys. Lett.* **2020**, 117, 063103.
- 35. Yang, D.-S.; Zewail, A. H. Ordered water structure at hydrophobic graphite interfaces observed by 4D, ultrafast electron crystallography, *Proc. Natl. Acad. Sci. U.S.A.* **2009**, 106, 4122-4126.
- 36. Yang, D.-S.; He, X. Structures and ultrafast dynamics of interfacial water assemblies on smooth hydrophobic surfaces, *Chem. Phys. Lett.* **2017**, 683, 625-632.
- 37. Wei, Z.; Chen, Y.; Dames, C. Negative correlation between in-plane bonding strength and cross-plane thermal conductivity in a model layered material, *Appl. Phys. Lett.* **2013**, 102, 011901.
- 38. Wang, Z.; Cahill, D. G.; Carter, J. A.; Koh, Y. K.; Lagutchev, A.; Seong, N.-H.; Dlott, D. D. Ultrafast dynamics of heat flow across molecules, *Chem. Phys.* **2008**, 350, 31-44.
- 39. Losego, M. D.; Grady, M. E.; Sottos, N. R.; Cahill, D. G.; Braun, P. V. Effects of chemical bonding on heat transport across interfaces, *Nat. Mater.* **2012**, 11, 502-506.

Supporting Information

Order-determined structural and energy transport dynamics in solidsupported interfacial methanol

Xing He, Ding-Shyue Yang*

Department of Chemistry, University of Houston, Houston, Texas 77204 United States

^{*}To whom correspondence should be addressed. Email: yang@uh.edu

1. Experimental Section

Preparation of methanol thin films with the 2D and 3D structural orders has been described in a previous report. S1 InAs(111) was chosen as the supporting substrate because its hydrophobic surface allows reliable preparation of the 2D- and 3D-ordered methanol assemblies, likely as a result of no significant interfacial interaction and very low surface roughness to interfere with the assembly growth. Experimentally, single-crystalline InAs(111)A substrates with a low surface roughness (<5 Å) were purchased from MTI Corporation. Prior to molecular depositions, InAs(111)A was sputtered by 1.5 keV Ar⁺ ions to remove surface oxides and contaminants. The surface quality and smoothness were confirmed by the clear streak patterns using reflection electron diffraction (Figure 1a). In an ultrahigh vacuum of the order of 10^{-10} torr, the surface temperature of the substrate was lowered to ≤100 K for molecular depositions. Thickness of a methanol film was determined by the effusion time used at a constant backing pressure in a molecular beam doser, whose deposition rate was calibrated by interferometry with a 515-nm laser beam. S1 As-deposited films were amorphous at ~100 K and produced diffuse scattering in the diffraction pattern (Figure 1b). By raising the substrate temperature slowly and annealing thin films at different temperatures, the two methanol assembly structures can be obtained (Figure 1, c and d).

The apparatus for UED in the reflection geometry has been described elsewhere. Here, photoexcitation of supporting InAs(111)A was achieved by the fundamental output of a regenerated amplified laser system (1030 nm, i.e. 1.20 eV which is sufficient to overcome the 0.35-eV band gap, with a pulse width of 170 fs); the repetition rate used was 2 kHz. The footprint of the excitation beam on the specimen surface was about 500 μm in the full width at half-maximum (FWHM). The pulsed electron beam was photogenerated from a cooled LaB6 emitter by the fourth harmonic of the fundamental (257 nm) and directed toward the specimen surface at a grazing incidence of ~1.0°, resulting in a footprint of 860 μm (15 μm) in FWHM along (perpendicular to) the propagation direction. At less than 1000 electrons per pulse, the instrumental response time was about 5 ps due to the temporal mismatch at a low incidence angle of electrons; however, this is sufficient for the observation of energy transport dynamics reported in this study. During the UED measurements, the thickness of a methanol film was monitored by laser interferometry to ensure no evaporation loss. Each diffraction frame at a given delay time for a certain film thickness was averaged from multiple rounds of image

acquisition produced by a total of about 10⁹ electrons. Hence, the stability and reproducibility of the results were also confirmed from the large number of time scans.

2. Simulation of thermal diffusion across the solid-molecule interface and in a methanol assembly

The photon energy ($E_{\rm ph}=1.2~{\rm eV}$ at 1030 nm) used to photoexcite is much greater than the bandgap of InAs ($E_{\rm g}=0.41~{\rm eV}$ at 100 K); ^{S3} hence, a major fraction of the absorbed photon energy will be released to the lattice as thermal energy, compared to other semiconductors such as silicon or GaAs with a bandgap greater than 1 eV and an orders-of-magnitude lower absorption coefficient. As a first-order approximation, we consider the early-time carrier-phonon coupling and the above-gap excess energy, $E_{\rm ph}-E_{\rm g}$ per electron-hole pair, to cause a lattice thermal impulse, assuming the photocarriers are long-lived. The actual average energy provided by each pair of carriers to the lattice may be slightly reduced because of the band-filling effect toward the thermalized Fermi-Dirac distribution across the bandgap. On the other hand, it is also probable that additional energy may be released by carriers that go through nonradiative relaxation via, e.g., an Auger process and/or defect-assisted decay at early or later times, considering the high carrier densities used in the present study. In either scenario or even a combined one with both effects, the following model remains largely the same except for $(E_{\rm ph}-E_{\rm g})/E_{\rm ph}$, the ratio of energy available to the lattice, which has no major influence on the temporal behavior that is the main observation of the present work.

Given the few-ps time scale for energy transfer by carrier–phonon coupling (and the probable ultrafast carrier annihilation processes at early times), the absorbed laser energy may be simply treated as a heating source in view of the time scale of 100s ps to few ns relevant to this work. The picture of thermalization after several up to few 10s of ps has been shown in various ultrafast structural studies, including photoexcitation of metals, S4-S6 semiconductors, and 2D materials, S8-S10 as well as further support by time-resolved x-ray diffraction in ns times. Therefore, the effective temperature in the InAs substrate may be modeled using the heat conduction equation, with the laser heating in the volume generation model: S13

$$\Delta T(z,t) = \int_{-\infty}^{t} dt' \frac{F(1-R)\alpha\kappa}{2\kappa} \times \frac{(E_{\rm ph}-E_{\rm g})}{E_{\rm ph}} \times \exp\left[-\left(\frac{t'}{\tau}\right)^{2}\right] \times \left[\exp\left[-\alpha z + \kappa\alpha^{2}(t-t')\right] \operatorname{erfc}\left(\frac{-z+2\kappa\alpha(t-t')}{2\sqrt{\kappa(t-t')}}\right) + \exp\left[\alpha z + \kappa\alpha^{2}(t-t')\right] \operatorname{erfc}\left(\frac{z+2\kappa\alpha(t-t')}{2\sqrt{\kappa(t-t')}}\right)\right], (S1)$$

where $\Delta T(z,t)$ is the temperature increase at the depth z beneath the substrate surface at time t; F the average laser fluence, R=0.337 and $\alpha=1.4758\times10^4$ cm⁻¹ the reflectivity and absorption coefficient of InAs at 1030 nm, respectively, and K=1.3 W/(cm·K) and K=1.27 cm²/s the thermal conductivity and diffusivity of InAs at 100 K, respectively, and K=1.27 cm²/s the temporal width of the thermal impulse. Then to each temperature K=1.27 cm the out-of-plane component of the mean-square displacements (MSD) K=1.27 can be calculated based on the Debye model:

$$\langle u_{\perp}^2 \rangle = \frac{3\hbar^2 T}{\overline{m} k_{\rm B} \Theta_{\rm D}^2} \tag{S2}$$

where $\hbar = h/2\pi$ is the reduced Planck constant, \overline{m} the average atomic mass, $k_{\rm B}$ the Boltzmann constant, and $\Theta_{\rm D} = 300$ K the Debye temperature of InAs. S16 Thus, we obtain

$$\langle u_{\perp,\text{InAs}}^2(z,t)\rangle = 1.71 \times 10^{-5} T(z,t) \,\text{Å}^2.$$
 (S3)

At the InAs-methanol interface, the increment of the average vertical displacement of a methanol molecule is presumed to be equal to that of the InAs surface atoms following laser excitation, considering them in a van der Waals contact:

$$\Delta(\langle u_{\perp,\rm M}^2(0,t)\rangle^{1/2}) = \Delta(\langle u_{\perp,\rm InAs}^2(0,t)\rangle^{1/2}) = \sqrt{1.71\times 10^{-5}} \left(\sqrt{T(0,t)} - \sqrt{T_0}\right), \tag{S4}$$

where T_0 is the base temperature of InAs and the supported methanol assembly prior to laser excitation. Hence, for the interfacial methanol molecules with small MSD increase,

$$\langle u_{\perp,M}^2(0,t)\rangle \cong \left[\langle u_{\perp,M}^2\rangle_{T_0}^{1/2} + \Delta\langle u_{\perp,M}^2(0,t)\rangle^{1/2}\right]^2.$$
 (S5)

Using Equation S2, we can derive the effective temperature of the interfacial methanol molecules $T_{\rm M}(0,t)$ from the vertical component of the molecular MSD $\langle u_{\perp,\rm M}^2(0,t)\rangle$,

$$\langle u_{\perp,M}^2(0,t)\rangle = \frac{3\hbar^2 T_{\rm M}(0,t)}{m_{\rm M} k_{\rm B} \Theta_{\rm D,M}^2} = 4.04 \times 10^{-4} T_{\rm M}(0,t) \,\text{Å}^2$$
 (S6)

with $m_{\rm M}$ being the mass of a methanol molecule and $\Theta_{\rm D,M} = 106$ K the Debye temperature of solid methanol. S17

With $T_{\rm M}(0,t)$ for the interface, the temperature of a methanol thin film at a distance $z_{\rm M}$ above the substrate surface can be calculated by the following one-dimensional thermal diffusion equation,

$$\frac{\partial^2 T_{\mathbf{M}}(z_{\mathbf{M}},t)}{\partial z_{\mathbf{M}}^2} - \frac{\rho_{\mathbf{M}} c_{\mathbf{p},\mathbf{M}}}{K_{\mathbf{M}}} \frac{\partial T_{\mathbf{M}}(z_{\mathbf{M}},t)}{\partial t} = 0$$
 (S7)

where $\rho_{\rm M}=1.015~{\rm g/cm^3}$ is the density of crystallized methanol, $c_{\rm p,M}=1.34~{\rm J/(g\cdot K)}$ the specific heat, $c_{\rm p,M}=1.34~{\rm J/(g\cdot K)}$ the thermal conductivity of methanol at 100 K. The

initial and boundary conditions are given below,

$$T_{\mathbf{M}}(z_{\mathbf{M}},0) = T_{\mathbf{0}} \tag{S8}$$

$$T_{\rm M}(0,t) = \frac{\left[\sqrt{4.04 \times 10^{-4} T_0} + \sqrt{1.71 \times 10^{-5} \left(\sqrt{T(0,t)} - \sqrt{T_0}\right)}\right]^2}{4.04 \times 10^{-4}}.$$
 (S9)

At the top of the methanol film, there should be no energy flow across the methanol-vacuum interface, thus

$$\left. \frac{\partial T_{\mathbf{M}}(z_{\mathbf{M}},t)}{\partial z_{\mathbf{M}}} \right|_{z_{\mathbf{M}}=d} = 0 \tag{S10}$$

where *d* is the film thickness. Thus, our model uses the physical constants of the materials involved. A good agreement between the experimental observations and the simulation results is reached when a universal factor of 1.2 is introduced to multiply all of the calculated temperatures (or 0.92 if 100% of the absorbed photon energy is released to the lattice at early times). Such a universal factor is likely due to certain experimental uncertainties including the actual sizes and overlap of the laser and electron footprints (particularly, the small vibrations of the liquid-nitrogen-cooled cryostat causing the coupled manipulator and sample holder to oscillate vertically, which affects the location of the footprint of grazing electrons), as well as a possible nonlinear response of the diffraction change to the laser fluence used (which will be further examined in a future study). A comparison between the nominal film thicknesses determined by laser interferometry and the values of *d* for best theoretical agreement is given in Table S1.

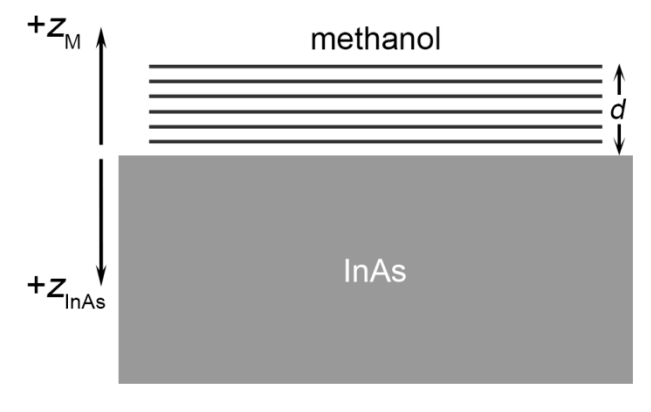


Figure S1. Schematic diagram for the InAsmethanol system considered in the thermal diffusion simulation. The positive *z* direction for each component is indicated. A set of boundary and initial conditions is presumed at the InAsmethanol interface, whereas another boundary condition is considered at the methanol—vacuum interface.

Table S1. Comparison of the interferometry-determined thicknesses of 2D-layered methanol films with the values used in the simulation for best match. The time when $ln(I/I_0)$ reaches a plateau (t_{max}) in the simulation for each thickness is also given.

Experimental nominal thickness (nm)	10	17	23	41
t _{max} (ps)	380	1100	>2000	> 2000
Thickness in simulation (nm)	10	17	22	41

Lastly, we note that another possible boundary condition other than Equation S4 may be considered at the solid-molecule interface for equal temperatures at all times,

$$T_{\rm M}(0,t) = T(0,t).$$
 (S11)

Although Equation S11 may seem reasonable, the simulation results yield effective temperature increases at the top methanol layer to be ~6.7 times of those derived from the experimental observations (or equivalently, a value of 0.15 much lower than 1 for the aforementioned adjustable parameter for multiplication), even though the temporal behavior agrees well. Thus, Equation S4 is found to be better supported, which also allows the microscopic picture of similar MSD at the interface. Furthermore, at the excitation fluence of 41.6 mJ/cm², the temperature at the top of the 10-nm-thick methanol film reaches up to 140 K (Figure 3), which is generally below the thermodynamics level for significant evaporation loss. S1 This is also consistent with the experimental finding that too high of a laser fluence would cause the loss of a methanol film over time as determined by interferometry.

3. Exclusion of Transient Surface Electric Fields as Possible Cause for Diffraction Changes

For ultrafast electron diffraction in the reflection geometry, it is crucial to examine that no significant effect is resulted from laser-induced transient electric fields above the surface of a photoexcited material. Our conclusion of negligible interference is reached by a number of observations. First, no major profile and intensity change is found around the shadow edge region of diffraction images (Figure 2a), which is a good indicator for the lack of significant transient electric fields. In contrast, shifts in the electron beam propagation can be clearly seen when surface electric fields are present. Second, the experimentally observed linear relation between $\ln(I_0/I)$ and s_{\perp}^2 agrees well with the structurally originated Debye-Waller effect

(Figure 2b), which cannot be explained by the presence of transient electric fields. If the observed diffraction changes were caused by transient electric fields, we would have anticipated more influence near the substrate surface (for electrons whose outgoing take-off angles are smaller, i.e. lower s_{\perp}^2) than farther away from the surface (for electrons with larger take-off angles, i.e. higher s_{\perp}^2). This would be completely opposite to our observations. Third, no difference would have been anticipated between 2D-layered and 3D-ordered nanoscale assemblies, should transient electric fields be the driving force for the observed dynamics. Thus, we conclude that our observation of diffraction changes is indeed of a structural origin and not by some Coulombic effects.

Reference:

- S1. He, X.; Wu, C.; Yang, D.-S. Communication: No guidance needed: Ordered structures and transformations of thin methanol ice on hydrophobic surfaces, *J. Chem. Phys.* **2016**, 145, 171102.
- S2. He, X.; Punpongjareorn, N.; Liang, W.; Lin, Y.; Chen, C.; Jacobson, A. J.; Yang, D.-S. Photoinduced strain release and phase transition dynamics of solid-supported ultrathin vanadium dioxide, *Sci. Rep.* **2017**, 7, 10045.
- S3. Zollner, S.; Gopalan, S.; Cardona, M. The temperature dependence of the band gaps in InP, InAs, InSb, and GaSb, *Solid State Commun.* **1991,** 77, 485-488.
- S4. Schäfer, S.; Liang, W.; Zewail, A. H. Structural dynamics of nanoscale gold by ultrafast electron crystallography, *Chem. Phys. Lett.* **2011**, 515, 278-282.
- S5. Tinnemann, V.; Streubühr, C.; Hafke, B.; Kalus, A.; Hanisch-Blicharski, A.; Ligges, M.; Zhou, P.; Linde, D. v. d.; Bovensiepen, U.; Hoegen, M. H.-v. Ultrafast electron diffraction from a Bi(111) surface: Impulsive lattice excitation and Debye–Waller analysis at large momentum transfer, *Struct. Dyn.* **2019**, 6, 035101.
- S6. Witte, T.; Frigge, T.; Hafke, B.; Krenzer, B.; Hoegen, M. H.-v. Nanoscale interfacial heat transport of ultrathin epitaxial hetero films: Few monolayer Pb(111) on Si(111), *Appl. Phys. Lett.* **2017**, 110, 243103.
- S7. Yang, D.-S.; Gedik, N.; Zewail, A. H. Ultrafast electron crystallography. 1. nonequilibrium dynamics of nanometer-scale structures, *J. Phys. Chem. C* **2007**, 111, 4889-4919.
- S8. Mannebach, E. M.; Li, R.; Duerloo, K. A.; Nyby, C.; Zalden, P.; Vecchione, T.; Ernst, F.;

- Reid, A. H.; Chase, T.; Shen, X.; Weathersby, S.; Hast, C.; Hettel, R.; Coffee, R.; Hartmann, N.; Fry, A. R.; Yu, Y.; Cao, L.; Heinz, T. F.; Reed, E. J.; Dürr, H. A.; Wang, X.; Lindenberg, A. M. Dynamic structural response and deformations of monolayer MoS₂ visualized by femtosecond electron diffraction, *Nano Lett.* **2015**, 15, 6889-6895.
- S9. Hu, J.; Vanacore, G. M.; Cepellotti, A.; Marzari, N.; Zewail, A. H. Rippling ultrafast dynamics of suspended 2D monolayers, graphene, *Proc. Natl. Acad. Sci. U.S.A.* **2016**, 113, E6555-E6561.
- S10. Lin, M.-F.; Kochat, V.; Krishnamoorthy, A.; Bassman, L.; Weninger, C.; Zheng, Q.; Zhang, X.; Apte, A.; Tiwary, C. S.; Shen, X.; Li, R.; Kalia, R.; Ajayan, P.; Nakano, A.; Vashishta, P.; Shimojo, F.; Wang, X.; Fritz, D. M.; Bergmann, U. Ultrafast non-radiative dynamics of atomically thin MoSe₂, *Nat. Commun.* **2017**, 8, 1745.
- S11. Shayduk, R.; Vonk, V.; Arndt, B.; Franz, D.; Strempfer, J.; Francoual, S.; Keller, T. F.; Spitzbart, T.; Stierle, A. Nanosecond laser pulse heating of a platinum surface studied by pump-probe X-ray diffraction, *Appl. Phys. Lett.* **2016**, 109, 043107.
- S12. Shayduk, R.; Gaal, P. Transition regime in the ultrafast laser heating of solids, *J. Appl. Phys.* **2020**, 127, 073101.
- S13. Bechtel, J. H. Heating of solid targets with laser pulses, J. Appl. Phys. 1975, 45, 1585.
- S14. Adachi, S. Optical dispersion relations for GaP, GaAs, GaSb, InP, InAs, InSb, $Al_xGa_{1-x}As$, and $In_{1-x}Ga_xAs_vP_{1-y}$, *J. Appl. Phys.* **1989**, 66, 6030-6040.
- S15. Le Guillou, G.; Albany, H. J. Phonon Conductivity of InAs, *Phys. Rev. B* **1972**, 5, 2301-2308.
- S16. Sirota, N. N.; Antyukhov, A. M.; Novikov, V. V.; Fyodorov, V. A. Thermodynamic functions of (InP)_x(InAs)_{1-x} from 5 to 300 K, *Cryst. Res. Technol.* **1982,** 17, 279-287.
- S17. Korolyuk, O. A.; Krivchikov, A. I.; Sharapova, I. V.; Romantsova, O. O. Heat transfer in solid methyl alcohol, *Low Temp. Phys.* **2009**, 35, 290-293.
- S18. Kirchner, M. T.; Das, D.; Boese, R. Cocrystallization with acetylene: molecular complex with methanol, *Cryst. Growth Des.* **2008**, 8, 763-765.
- S19. Sugisaki, M.; Suga, H.; Seki, S. Calorimetric study of the glassy state. III. novel type calorimeter for study of glassy state and heat capacity of glassy methanol, *Bull. Chem. Soc. Jpn.* **1968**, 41, 2586-2591.
- S20. Li, J.; Wang, X.; Chen, Z.; Zhou, J.; Mao, S. S.; Cao, J. Real-time probing of ultrafast residual charge dynamics, *Appl. Phys. Lett.* **2011**, 98, 011501.